Journal of Catalysis 413 (2022) 517–526

Contents lists available at ScienceDirect

Journal of Catalysis

journal homepage: www.elsevier.com/locate/jcat

Revealing the roles of hydrocarbon pool mechanism in ethanol-to-hydrocarbons reaction

Shu Zeng [a,b,1], Wenna Zhang [a,1], Junjie Li [c], Shanfan Lin [a,b], Shutao Xu [a,*], Yingxu Wei [a], Zhongmin Liu [a,b,c]

[a] National Engineering Research Center of Lower-Carbon Catalysis Technology, Dalian National Laboratory for Clean Energy, iChEM (Collaborative Innovation Center of Chemistry for Energy Materials), Dalian Institute of Chemical Physics, Chinese Academy of Sciences, Dalian 116023, PR China
[b] University of Chinese Academy of Sciences, Beijing 100049, PR China
[c] State Key Laboratory of Catalysis, Dalian Institute of Chemical Physics, Chinese Academy of Sciences, Dalian 116023, PR China

ARTICLE INFO

Article history:
Received 1 April 2022
Revised 12 June 2022
Accepted 1 July 2022
Available online 4 July 2022

Keywords:
Ethanol-to-hydrocarbons
In-situ ssNMR
ZSM-5 zeolite
Reaction mechanism

ABSTRACT

Ethanol-to-hydrocarbons (ETH) process, is investigated in this work due to the requirement of sustainable production route for light olefins such as ethene and propene. Majority of the mechanism insights of ETH process are principally proposed based on the methanol-to-hydrocarbons (MTH) process, which involves a homologous reaction system. The reaction intermediate species including cyclopentenyl cations and aromatics species, which are denoted as "hydrocarbon pool (HCP)" species in MTH process, were discovered and identified in the ETH process by *in situ* solid-state ^{13}C NMR (ssNMR) experiments, advanced 2D ^{13}C–^{13}C INADEQUATE (Incredible Natural Abundance DoubIE QUAntum Transfer Experiment) ssNMR experiment, $^{12}C/^{13}C$-C_2H_5OH isotope switching experiments complemented by gas chromatography-mass spectroscopy (GC–MS). Especially, in the ETH reaction, ethylcyclopentenyl cations and their deprotonated form were first captured and exhibited relatively higher activity in the formation of ethene and propene. Multi-routes with the participation of these active intermediates were proposed and evaluated by density functional theory calculation (DFT), demonstrating that they can play important roles in the formation of olefins. Ethene formation are mainly formed from ethanol dehydration, whereas propene can be produced via multi-routes with the participation of the captured HCP species. Moreover, the detailed reaction routes may be modulated by the temperature. This work provides direct evidences of the critical function of HCP species in the ETH process and reveals the mechanism of olefin formation.

1. Introduction

Ethanol-to-hydrocarbons (ETH) process catalyzed over zeolite catalysts has recently attracted extensive attentions from both academia and industry due to the massive resources from bioethanol production and coal-to-ethanol process [1–3]. A great deal of work on industrial development and fundamental understanding on the zeolite-catalyzed ETH process have been done, however, mainly focus on catalyst modification [4–6] and products optimization [7,8]. At present, there is not a unified understanding on reaction mechanism, which remains a controversial topic [9–11]. It is noteworthy that majority of the mechanism insights are principally based on the understanding of its homologous reaction, methanol-to-hydrocarbons (MTH) process, which is performed over similar zeolite catalyst and presents the close product distributions as ETH process [12]. The MTH reaction mechanism has been systematically investigated by both experiment [13–18] and theory [19–21] for many years, including complex reaction process, reaction intermediates and catalytic routes. Inspired by this, the ETH process was supposed to have similar mechanism to the "sister-reaction" (MTH process) [22–24]. For instance, the ethoxy [25,26] and triethyloxonium ion (TEO) [27] in ethanol dehydration reaction corresponding to the methoxy and trimethyloxonium ion (TMO) in methanol dehydration stage, were observed by infrared (IR) and solid-state nuclear magnetic resonance (ssNMR) spectroscopies directly, and play an important role as initial active species. However, it is imperative to note that the detailed reaction mechanism of ETH process should not be considered exactly identical to MTH process. As the ETH process starts with a C_2 reactant, the formation of the initial carbon–carbon bonds, still an ongoing controversy in the MTH process, is not interfered in this reaction. Furthermore, as the coupling of ethanol molecules which have even carbon number occurs in ETH process, it will be hard to shed light on the formation of the products and intermediates with the odd carbon number, especially propene.

* Corresponding author.
E-mail address: xushutao@dicp.ac.cn (S. Xu).
[1] These authors contributed equally.

https://doi.org/10.1016/j.jcat.2022.07.002
0021-9517/

Up to now, three different mechanisms have been proposed for the ETH process, including the acid-catalyzed mechanism [28], the radical-intermediate mechanism [29] and the dual cycle mechanism [12]. It was inclined to consider that ethanol first dehydrates to generate an ethene intermediate, which subsequently transforms to C_{3+} hydrocarbons and aromatics via secondary reactions, such as oligomerization, cyclization, aromatization and cracking as in the process of MTH [3,9,30]. Zhou et al have done an elaborate work on the dehydration of ethanol to ethene, the triethyloxonium ion (TEO) mediated reaction pathway was supposed to be more energetically favorable compared to the ethoxy precursors. During the secondary stage of ETH reaction, three kinds of ethyl-substituted benzene species were identified and responsible for the formation of ethene in the work of Chowdhury et al. [10]. And they hold the view that the olefins-based cycle is deficient in ETH process due to the failure in capture of olefinic-hydrocarbon pool (HCP) species [10], which is controversial to the previous conclusion [9,12]. Although they have exhibited these exquisite works to readers, the whole conversion process of ethanol was rarely observed by any *in situ* technology. In addition, the detailed active intermediates and explicit production paths of light olefins, especially propene, are still not fully given.

Focused on the dehydration stage of ethanol, our teams recently reported different surface species on ZSM-5 zeolite, including adsorbed ethanol with side-on and end-on orientation, diethyl ether with adsorbed and activated state, ethoxy, TEO and even cyclopentadienyl cations, the evolution process of these captured intermediates was also exhaustively illustrated [31]. Carbocations which are demonstrated as critical active intermediates and contributed to the formation of ethene and propene via a dual-cycle mechanism (olefins-based and aromatics-based cycles) and a complementary cyclopentadienes-based cycle mechanism in MTH process [32–34], are rarely identified in ETH process. Furthermore, the important roles and explicit structure of these cations in ETH process have not been reported yet. Therefore, it is worth for us to investigate whether these critical carbocations and the corresponding catalytic cycles mentioned in the MTH process are universal in alcohol conversion. The active intermediates and exact reaction pathway in ETH process should be further revealed.

Herein, multiple methods like magic angle spinning (MAS) solid-state nuclear magnetic resonance (ssNMR), gas chromatography-mass spectroscopy (GC–MS), and $^{12}C/^{13}C$-ethanol isotope switching experiments were performed to investigate the issues mentioned above, including the reaction pathway of ETH process, capture and identification of the active intermediates on the working catalyst as shown in Scheme 1. Some critical intermediates, ethyl-substituted carbocations, especially ethylcyclopentenyl cations and ethyl-substituted benzene species were identified, and the feasibility and the contribution on the production of the target products like ethene and propene were investigated by density functional theory (DFT) calculation. Except for the direct dehydration of ethanol to form ethene, the triple-cycle mechanism including olefins-based cycle, aromatics-based cycle, and cyclopentadienes-based cycle was demonstrated to be feasible in ETH process for generating olefins, especially propene. In addition, the contribution of the proposed reaction routes is susceptible to temperature.

2. Experimental

2.1. Catalyst and characterizations

The H-ZSM-5 zeolite used in this work was synthesized by a seed surface crystallization method described in reference [35]. Firstly, the nano silicalite-1 was synthesized as a seed. 7 g of TPAOH solution (25 wt% in H_2O), 50 g of TEOS, and 30 g of H_2O were mixed and stirred at 308 K for 12 h, and then transferred into a 200 mL Teflon-lined steel autoclave and crystallized at 353 K for 72 h. The molar composition of the final gel was 1 TEOS:0.36 TPAOH:19 H_2O. Then, the ZSM-5 zeolite was prepared as following steps. 17.75 g of tetra-propyl ammonium bromide (TPABr) (17.75 g) and 66.67 g of silica sol (30 wt% in H_2O) were mixed at 308 K, then the seed was added into the silica gel. After stirring for 30 min, 3.32 g of $AlCl_3{\cdot}6H_2O$ and 45 g of H_2O was added dropwise into the silica gel. Then, 22.26 g of ethylamine aqueous solution (65 wt% in H_2O, as alkali source) was poured into the obtained silica-aluminum gel. Finally, the mother gel was transferred into a Teflon-lined stainless-steel autoclave and crystallized at 443 K for 72 h. The molar composition of the final gel was 1 SiO_2:0.02 Al_2O_3:0.20 TPABr:0.27 ethylamine:17 H_2O. H-ZSM-5 zeolite was obtained after calcination by removing the organic template. The catalyst characterizations, including powder X-ray diffraction (XRD) and scanning electron microscope (SEM) are showed in Supplementary Fig. S1-2.

2.2. Catalytic testing

Ethanol conversion experiments were performed in a continuous-flow fixed-bed tubular quartz reactor at atmospheric pressure, and the reaction temperature was monitored with a thermocouple in the catalyst bed. For the reactions at different temperatures, firstly 100 mg (40–60 mesh) H-ZSM-5 samples were purged at 500 °C under helium for 30 min, and then the reactor was cooled to the desired reaction temperature (100–450 °C). For the reaction with different WHSV conditions at 250 °C, 10–200 mg H-ZSM-5 samples (40–60 mesh) were diluted with variable weight (270–0 mg) quartz sand (40–60 mesh) to keep the same bed volume. Ethanol (Beijing J&K Scientific Co. Ltd., purity greater than 99.9%) was supplied by passing helium through saturation evaporator at 20 °C water bath. The effluent products were analyzed on online by gas chromatography (Agilent GC 7890A) equipped with a HP-PLOTQ capillary column, a FID detector, and a mass spectrometric detector (Agilent 7890A/5975C).

2.3. ssNMR experiments

All the solid-state NMR experiments were performed on a Bruker Avance III 600 spectrometer equipped with a 14.1 T wide-bore magnet. The resonance frequencies in this field strength were 119.2 MHz, 156.4 MHz and 150.9 MHz for ^{29}Si, ^{27}Al and ^{13}C, respectively. The ^{27}Al MAS NMR spectrum was recorded use a one pulse consequence with spinning rate of 12 kHz and 2 s recycle delay. The ^{29}Si MAS NMR spectrum was recorded with a high-power proton decoupling sequence with a spinning rate of 8 kHz and 10 s recycle delay. Chemical shifts of ^{27}Al spectrum was referenced to $Al(NO_3)_3$ solution at 0 ppm, and that of ^{29}Si spectrum was referenced to kaolinite at −91.5 ppm.

Prior to ^{13}C-ethanol reaction, the catalyst was dehydrated under the home-built vacuum line at 420 °C overnight. All the chemical shifts of ^{13}C NMR spectroscopies were referenced to adamantane with the up-field methine peak at 29.5 ppm.

The 2D INADEQUATE (Incredible Natural Abundance DoublE QUAntum Transfer Experiment) ssNMR experiment was conducted using the 4 mm WVT probe with the spinning rate of 14 kHz and recycle delay of 1 s. The $\pi/2$ pulse width of ^{13}C and ^{1}H used was 3.6 μs and 4.5 μs, respectively. The contact time was 3 ms for polarization transfer from ^{1}H to ^{13}C. The rotor synchronized τ delay in the INADEQUATE experiments was optimized to about 2.14 ms.

For the *in situ* ^{13}C ssNMR experiment under continuous-flow (CF) condition, about 200 mg of pre-dehydrated H-ZSM-5 was filled into a 7 mm NMR rotor reactor as a hollow cylinder with

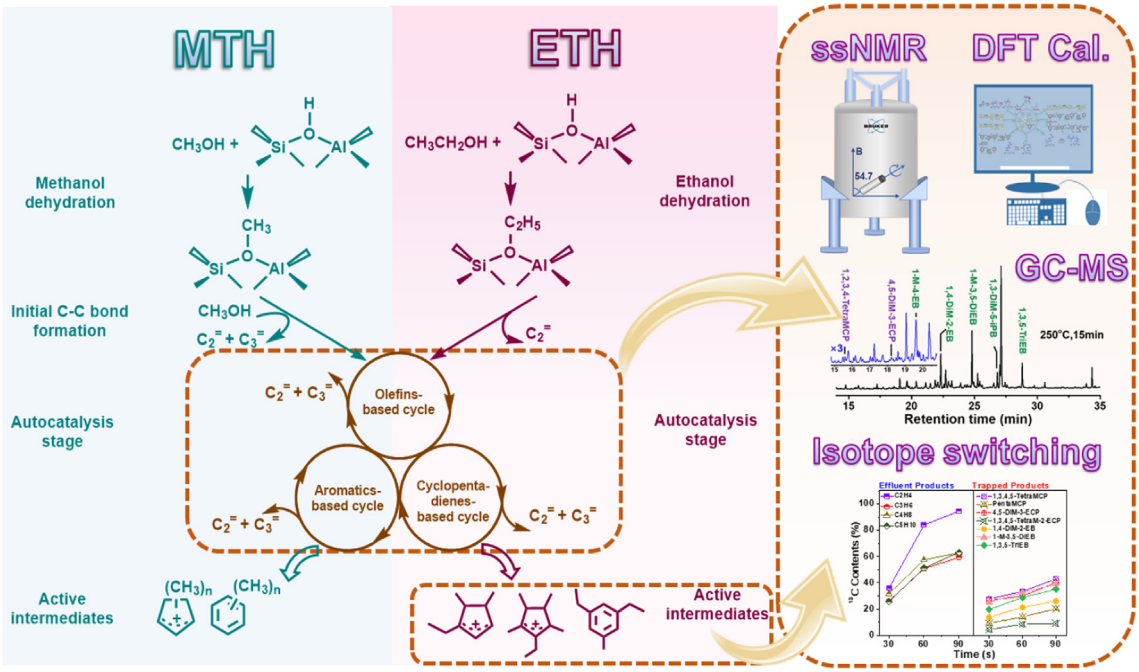

Scheme 1. Illustration and comparison of reaction mechanism of the thoroughly investigated methanol-to-hydrocarbons (MTH) process (highlighted in blue background) and ambiguous ethanol-to-hydrocarbons (ETH) process (highlighted in pink background). Several kinds of ethyl substituted cyclopentenyl cations and aromatics with high activity were identified by multiple technology in ETH process. Moreover, the triple-cycle mechanism that mediated by the identified species was proposed analogously to MTH process. In dotted frame on the right, multiple methods for unearthing the findings in this work are illustrated.

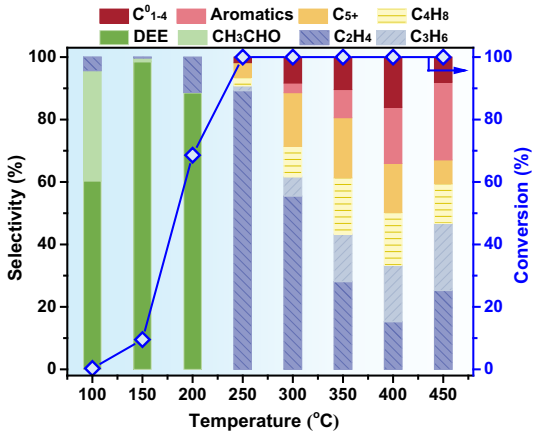

Fig. 1. The conversion and selectivity of products of the ethanol conversion on H-ZSM-5 zeolite at varied reaction temperature from 100 to 450 °C. DEE denotes diethyl ether, $C^0_{1\text{-}4}$ refers to the C_1-C_4 alkanes, C_{5+} refers to the aliphatic hydrocarbons with carbon number above five, including chain alkanes, cyclic alkanes, chain alkenes and cyclic alkenes, aromatics includes benzene, toluene, xylenes, ethylbenzene, methyl ethylbenzenes and trimethylbenzenes. (The effluent products were analyzed after reaction for 5 min at each temperature with the WHSV of 2 h^{-1}).

the assistance of a specially constructed tool in a nitrogen glove box. Before the introduction of ethanol, the catalyst was activated at 300 °C for 30 min under flowing helium (36.5 mL/min), and then the temperature was adjusted to the desire reaction temperature. Subsequently, continuous-flow $^{13}CH_3^{13}CH_2OH$ was fed into the 7 mm NMR rotor by passing the carrier gas He through an ethanol saturator kept at 10 °C with a WHSV of 0.5 h^{-1}, and ^{13}C MAS NMR spectra were recorded using one pulse sequence with a spinning rate of 3355 Hz simultaneously. In order to obtain the ^{13}C MAS NMR spectra with better signal-to-noise ratios, 0.5, 2 and 4 s recycle delay was used during the periods from 0 to 10 min, 10 to 30 min and 30 to 74 min, respectively. After the *in situ* CF ^{13}C ssNMR experiment, the sample was removed from the 7 mm rotor and transferred into a 4 mm rotor at room temperature for the ^{13}C CP/MAS experiment. The spinning rate of 12 kHz, recycle delay of 2 s and contact time of 3 ms was used for the CP sequence.

For the *in situ* ^{13}C ssNMR experiments under batch-like condition, about 20 kPa of $^{13}CH_3^{13}CH_2OH$ saturated vapor was adsorbed in pre-dehydrated H-ZSM-5 zeolite at 20 °C and keep equilibrium for 30 min, then evacuated 1 min to remove the supersaturated ethanol from the zeolite surface. According to the equation of state of ideal gas (PV = nRT), the amount of the ethanol is 3.53×10^{-4} mol. The elementary composition of the used H-ZSM-5 zeolite is $Si_{0.156}Al_{0.006}O_{0.331}$ according to XRF analysis (quality ration). Therefore, the amount of the Al content can be obtained from the following formula:

$$n(Al) = \frac{m(Al)}{M_{Al}} = \frac{0.006M_{Al} \times m_{cat.}/(0.156M_{Si} + 0.006M_{Al} + 0.331M_O)}{M_{Al}} \quad (1)$$

Which is 1.20×10^{-4} mol. Therefore, about 2.9 ethanol adsorbed on one Al site can be obtained in this sample. Subsequently, about 80 mg H-ZSM-5 zeolite that adsorbed ethanol was transformed into a 4 mm NMR rotor reactor, and the sample was quickly heated to 217 °C in the 4 mm H-X probe. Meanwhile, the *in situ* ^{13}C CP/MAS NMR spectra were recorded continuously to present the conversion process of ethanol with the spinning rate of 10 kHz. 1 and 2 s recycle delay was used during the periods from 0 to 44 min and 44 to 64 min, respectively. 3 ms contact time was used for this experiment.

The temperature of the probe mentioned above were calibrated using KBr as a heat indicator, according to the change of the chemical shift form ^{79}Br MAS NMR spectra under different temperatures. The ^{79}Br chemical shifts are linearly related to temperature with a slope of −0.0249 ppm/K [36]. The chemical shift is set to 0.0 ppm at 293 K. Therefore, the real-time temperature (T_{real}) of

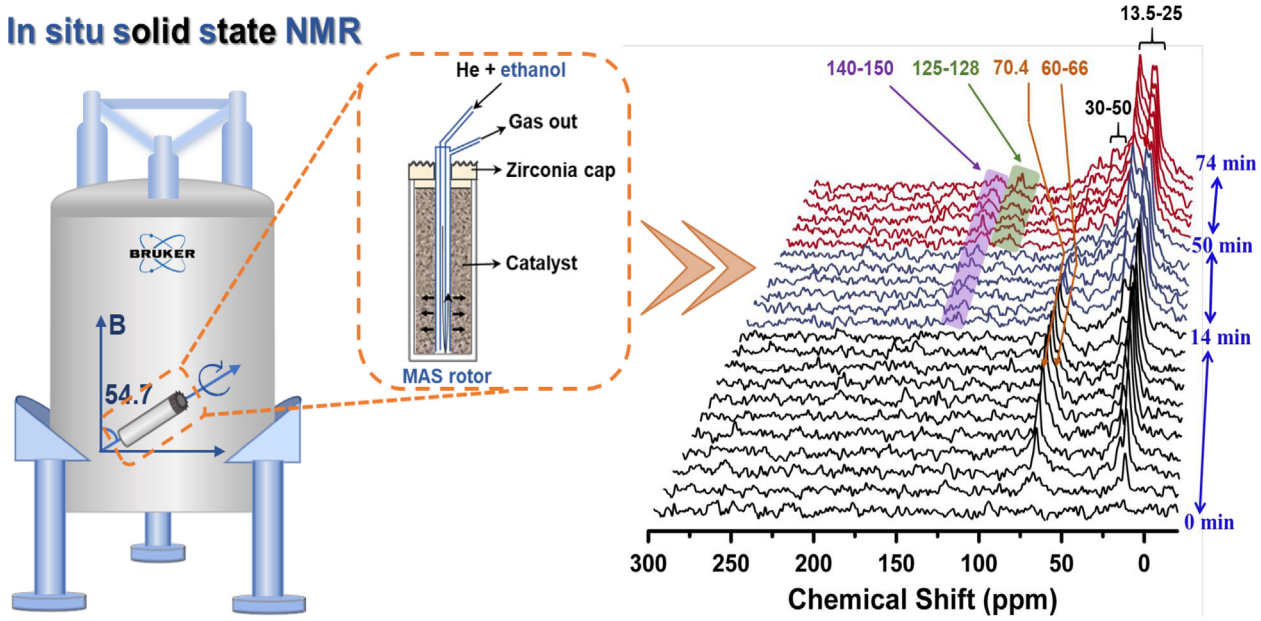

Fig. 2. In situ ^{13}C MAS NMR spectra of the continuous-flow ethanol conversion on H-ZSM-5 zeolite at 258 °C and WHSV of 0.5 h^{-1}. The reaction was conducted on the 7 mm MAS-CAT probe with a spinning rate of 3355 Hz. The temperature of the probe was calibrated by potassium bromide (KBr). The spectra were recorded every 30 s from 0 to 10 min, then every 2 min from 10 to 30 min, and finally every 4 min from 30 to 74 min.

sample can be deduced by the following equation, where δ represent to the chemical shift of KBr at the actual temperature.

$$T_{real} = 293 - \delta/0.0249 \quad (2)$$

2.4. $^{12}C/^{13}C$-methanol switch experiment

In the $^{12}C/^{13}C$-ethanol switch experiment, ^{12}C-ethanol was firstly introduced into reactor by passing He through saturation evaporator maintained at 20 °C at designated temperature (eg. 250 °C, 350 °C and 450 °C in this work) for 15 min. Then the feeding of ^{12}C-ethanol was stopped and ^{13}C ethanol (fed by passing the carrier gas helium through a $^{13}CH_3{}^{13}CH_2OH$ saturator with same flow rate) was switched into the reactor for 30, 60 and 90 s respectively. Subsequently, sufficient liquid nitrogen was used to cool the catalyst very quickly to stop the reaction. The isotopic distribution of effluents and the materials confined in the catalyst was analyzed using an Agilent 7890A/5975C GC/MSD.

2.5. Confined organics determination with GC–MS

The catalysts that after reaction were dissolved in 20% hydrofluoric acid solution to destroy the framework structure of zeolite and release the confined organics trapped in the channel of H-ZSM-5. Then, dichloromethane (CH_2Cl_2) with 100 ppm C_2Cl_6 as an internal standard was used to extract the confined organics. The organic phase was analyzed by Agilent 7890A/5975C GC/MSD equipped with an HP-5 capillary column.

2.6. Theoretical calculation for ETH reaction mechanism

Cluster model of ZSM-5 was extracted from the crystallographic MFI structure of the International Zeolite Association. As shown in Fig. S3, the 72 T model covers the intersection cavity between the straight channel and the zigzag channel, which can consider the interaction between the adsorbed species and the zeolite framework, as same as the periodic structure. It is large enough to account for the effects of the topological structure of the catalyst [37–38]. The terminal Si-H was fixed with the bond length of 1.47 Å oriented along the direction of the corresponding Si-O bond.

For the calculation model, the substituted Al atom was placed at the T12 site and Al12-O24H-Si12 site was chosen to represent the Brønsted acid site of H-ZSM-5 to evaluate the feasible pathway of ethanol conversion. T12 site has been proved as the reaction active site that is easy access by the bulk intermediates such as aromatics and cyclopentadienes species [37–38]. This site is located in the intersection of the straight channel and the sinusoidal channel of zeolite H-ZSM-5 and it has maximum reaction space, accessible to the adsorbed molecules.

In the 72 T cluster, the local structure of 24 T around the Al center and the adsorbed species were optimized, while the rest of atoms were fixed in the crystallographic data. Various adsorption structures and transition states (TS) were predicted at the ONIOM (ωB97XD/6-31G (d, p):AM1) level. The ωB97XD method, a long-range corrected hybrid DFT for dispersion developed by Chai and Head-Gordon, can describe long-range dispersion interactions on zeolites catalytic system. The wB97XD functional uses a version of Grimme's D2 dispersion model, which can reflect the weak van der Waals(vdW) interaction between the adsorbed organic species and the zeolite framework. The frequency calculations were performed at the same level as geometry optimizations. Only a single imaginary frequency was observed for the transition state, and no imaginary frequency was observed for the adsorbed state. Furthermore, on the basis of optimized structures, the single-point energies were calculated at the level of ωB97XD/6-31G (d, p). The energies have been corrected for zero-point vibration energies. All calculations were performed using the Gaussian 09 software package.

3. Results and discussion

3.1. Catalytic performance of ethanol conversion on H-ZSM-5 zeolite

The structural characterizations of H-ZSM-5 are described in the Supplementary Fig. S1-S5. The SEM image (Fig. S1), XRD pattern (Fig. S2) of the H-ZSM-5 zeolite show the regular crystal

morphology and good crystallinity with MFI structure. The ^{27}Al MAS NMR spectrum (Fig. S4) reveals the dominating tetra-coordinated framework aluminum species of the catalyst. The framework atomic ratio of silicon to aluminum (Si/Al) is 26.6 calculated from ^{29}Si MAS NMR spectrum (Fig. S5). The catalytic performance of ethanol conversion over H-ZSM-5 zeolite was evaluated at different temperature. The conversion and products distribution are presented on Fig. 1 with the temperature increase from 100 to 450 °C. A low conversion of ethanol is obtained at relatively low reaction temperatures (<250 °C), in which the dehydration of ethanol to diethyl ether (DEE) is the dominant reaction route, accompanied by a small amount of ethene and acetaldehyde. With reaction temperature increasing from 250 to 450 °C, the ethanol conversion reaches and stays at 100%. Significant amounts of olefins, alkanes and even aromatics appear in the products stream. It is noteworthy that the selectivity of products changes distinctly with the temperature increase from 250 to 450 °C and shows the following trends: (1) When the temperature goes up from 250 to 400 °C, the selectivity of ethene decreases from 89.2% to 15.2%, while the selectivity of C_{3+} products (including propene, butenes, C_{5+} products, C_{1-4} alkanes and aromatic products) show a continuous upward trend, which imply the promotion effect of the temperature for the further conversion of the produced ethene. (2) As the temperature rises further from 400 to 450 °C, the selectivity of ethene presents a recovery to 25.2%, while the selectivity of butenes, C_{5+} products and C_{1-4} alkanes experiences a modest decrease, which implies the polymerization of produced ethene is inhibited at higher temperature. C_{5+} refers to the aliphatic hydrocarbons with carbon number above five, including chain alkanes, cyclic alkanes, chain alkenes and cyclic alkenes as shown in Fig. S6.

Therefore, it can be deduced from the Fig. 1 that ethene may be mainly produced by the dehydration of ethanol. Increasing the temperature from 250 to 400 °C may promote secondary reactions of ethene and also accelerate the production of propene and other long chain olefins. It is obviously perceived that the product distribution is sensitive to the reaction temperature, presenting a temperature-modulated reaction route of ethanol conversion. However, it is still unknown about the detailed formation pathway of light olefins, especially propene. Further investigations are imperative to shed light on the reaction mechanism. The effluent products distribution of ethanol conversion on H-ZSM-5 varying with time-of-stream (TOS) at different temperature from 250 to 450 °C is explicitly presented on Fig. S7-S9. It is worthy to note that the selectivity of ethene shows a tendency of decreasing firstly and then increasing with temperature increase from low to high, corresponding to the variation of the selectivity of C_3-C_6. Therefore, it can be established that ethene can be produced firstly by ethanol dehydration, then some active intermediates like HCP species in MTH process may be generated via the secondary reaction of ethene, leading to a downward tendency of ethene selectivity at the temperature range of 250–400 °C. At relatively high temperature, dehydration becomes dominant again which cause the increase of ethene selectivity again. The decreasing tendency of ethene selectivity at the initial stage (<83 min) in Fig. S7 also demonstrated the formation and accumulation of some intermediates, while rising temperature will make this tendency less noticeable (Fig. S8-9). Changing the weight hour space velocity (WHSV) of the reaction at 250 °C, it also reveals the characteristics of the ethanol conversion with two stages as shown Fig. S10. Under high WHSV conditions that means shorter contact time between ethanol and catalyst (eg. 10–20 h^{-1}), ethanol exhibits incomplete conversion at 75.5%-61.6%. And the effluent products are only DEE and ethene which means secondary reaction of ethene is suppressed. Under low WHSV conditions (eg. 1–5 h^{-1}), except for the ethene, DEE and acetaldehyde, tiny amount of C_4 products can be obtained through the dimerization of the produced ethene. The appearance of C_{3+} products at low WHSV (eg. 1–5 h^{-1}) condition also means the secondary reaction of the ethene after the dehydration of ethanol. In this case, the whole reaction process, the nature and specific structure of the active species, as well as their possible catalytic routes need to be further revealed via experimental and theoretical investigations.

3.2. In situ ^{13}C MAS ssNMR experiments for the capture of active intermediates

To confirm the above speculation, the *in situ* ssNMR experiment with the continuous-flow (CF) $^{13}CH_3^{13}CH_2OH$ conversion was conducted in a rotor reactor at 258 °C. The real-time evolution of the ethanol conversion and the reaction intermediate species generation can be presented under real working conditions. Mild reaction conditions aim to lower the reaction rate and realize a possible capture of the active intermediates. The signals presented in the *in situ* ^{13}C MAS NMR spectra under continuous flow (CF) condition (Fig. 2) and the ^{1}H–^{13}C CP/MAS NMR spectra under batch-like condition (Fig. S11, Fig. S12) show the following signals: (1) 10–50 ppm from aliphatic groups; (2) 50–73 ppm from alkoxy groups; (3) 120–140 ppm from aromatic moieties; and (4) 140–150 ppm and 240–251 ppm from carbenium ions [39–40]. As shown in Fig. 2, the formation of diethyl ether (66 ppm) and ethoxy (70.4 ppm) from the reaction of ethanol (60 ppm) dehydration is clearly visible at the initial 10 min. Meanwhile, the appearance of these species is also evidenced in Fig. S11. After 14 min, the peaks in the 10–50 ppm range are more complex, suggesting that significant amounts of aliphatic hydrocarbons are produced. It can be deduced that the oligomerization of the produced ethene works efficiently during this period. Meanwhile, an eye-catching finding is that the occurrence of the signals at 125–128 and 140–145 ppm, the characteristic peaks of aromatics and cyclopentenyl cations respectively. Catalyst-trapped highly active cyclopentenyl cations, analogous to MTH process [13,41], are captured directly in *in situ* ETH reaction. Aromatic species (50 min) appears later than cyclopentenyl cations (16 min), indicating that the cyclopentenyl cations may be formed preferentially than aromatic species. The formation of cyclopentenyl cations is further consolidated by the *in situ* ^{1}H–^{13}C CP/MAS NMR spectra at 217 °C in the ethanol conversion under batch-like condition with the observation of the more pronounced peaks at 146–154 ppm and the relatively weak peaks at 240–250 ppm (shown in Fig. S11). Meanwhile, the characteristic peaks of the cyclopentenyl cations are kept in the ^{13}C CP/MAS NMR spectrum after the *in situ* CF ethanol reaction (Fig. S12), illustrating the relatively high stability of the captured intermediate species.

In summary, the evolution of the generated organic species over H-ZSM-5 in ETH reaction was clearly revealed by the *in situ* ssNMR spectroscopy. Firstly, ethanol experiences a dehydration stage to form DEE and ethoxy groups. Then, ethene could be eliminated from ethoxy groups. Thereafter, ethene quickly transforms to active cyclopentenyl cations via oligomerization and cyclization reactions. Direct observation of these cyclopentenyl cations under real conditions verified the formation of active intermediates like HCP species in ETH process, then aromatics could be also formed via H-transfer and aromatization reaction in the following steps. These observations are of great significance to clarify the ambiguous reaction mechanism of ethanol conversion.

3.3. Advanced 2D INADEQUATE ssNMR experiment for identifying the cations

To further identify the structure of the captured cyclopentenyl cations, advanced 2D INADEQUATE (Incredible Natural Abundance DoublE QUAntum Transfer Experiment) ssNMR experiment was

conducted in combination with GC–MS analysis. 2D INADEQUATE ssNMR experiment is based on exclusively J couplings and provides through-bond correlation information, making an unambiguous assignment for carbon–carbon (C-C) connectivity [42]. In the 2D spectrum, two individual ^{13}C frequencies in the single quantum (F2) dimension have common frequency in the double quantum (F1) dimension denotes the information that the two carbon atoms are directly bonded. $^{13}CH_3^{13}CH_2OH$ was used to ensure the high sensitivity of NMR signals and the accurate determination of the catalyst-trapped carbocations. In order to avoid the interference of polyalkyl aromatics to cyclopentenyl carbocations, the sample was reacted with ^{13}C-ethanol at 150 °C for 1 h to obtain more cyclopentenyl carbocations.

The spectrum in Fig. S13 shows multiple cross-peaks, reflecting the complexity of the confined cyclic organic species. For detailed information, the enlarged views of the Fig. S13 at different regions are shown in Fig. 3 with corresponding colors. Four cyclopentenyl cations with methyl or ethyl substitution are explicitly identified, which are 2,3,4,5-tetramethylcyclopentenyl cation (**I**), 1,2,5-trimethylcyclopentenyl cation (**II**), 2,3,4,5-tetramethyl-1-ethylcy clopentenyl cation (**III**) and 3,4-dimethyl-2-ethylcyclopentenyl cation (**IV**). For example, the 2,3,4,5-tetramethylcyclopentenyl cation **I** can be explicitly identified through the correlations of C2 (C5) (249 ppm)-C1 (146 ppm), C2 (C5) (249 ppm)–C3 (C4) (47 ppm), C2 (C5) (249 ppm)-C6 (C7) (24 ppm), C3 (47 ppm)-C4 (47 ppm) and C3 (C4) (47 ppm)-C8 (C9) (19 ppm) as marked in orange in Fig. 3. Similarly, the remaining three cyclopentenyl cations **II** (blue), **III** (crimson) and **IV** (green) are also identified with the same approach. Moreover, the identified four cyclopentenyl cations are further consolidated by the detection of their neutral form (i.e., cyclopentadienes) when analyzing the trapped organics extracted from the H-ZSM-5 after dissolving the ethanol-reacted catalyst (obtained after reaction at 250 °C for 15 and 30 min) by GC–MS (seen in Fig. S14). Meanwhile, several ethyl substituted-benzene species and long-chain olefins were also obtained in the confined species, such as 1-methyl-4-ethylbenzene, 1,4-dimethyl-2-ethylbenzene, 1,3,5-triethylbenzene, 1-methyl-3,5-diethylbenzene, 1,3-dimethyl-5-isopropylbenzene and 2,6-dimethly-2,4,6-octatriene (or it's isomers). Serving as reactive intermediates in MTH process, cyclopentenyl cations and polymethylbenzenyl cations were emphasized on their high activity and involvement in MTH reaction in numerous works [43–44]. In the present work, two ethylcyclopentenyl cations (**III**, **IV**) were firstly captured and identified in ETH process. Cyclopentenyl cations have been reported in MTH process as key HCP species to explain the production of ethene and propene[31]. In addition, the methylcyclopentadienes-based cycle has also been proposed as an alternative route in MTH process for the formation of light olefins [34]. For ETH reaction, ethanol as the starting reactant, it can be deduced that the ethylcyclopentenyl cations and ethyl substituted-benzenyl species are possibly formed through the ethylation of the cyclic organic species.

3.4. $^{12}C/^{13}C$-ethanol isotope switching experiments for demonstrating the reactivity of intermediate species

To confirm the participation of the obtained ethylcyclopentenyl cations and ethyl-substituted benzenyl species under working condition, $^{12}C/^{13}C$-ethanol isotope switching experiments were performed at a series of temperature (250, 350, and 450 °C) after ^{12}C-ethanol reaction for 15 min.

After switching the feeding of ^{12}C-ethanol to ^{13}C-ethanol ($^{13}CH_3^{13}CH_2OH$) for 30, 60, and 90 s, both the effluent and trapped products present the ^{13}C atom incorporation due to the interaction of $^{13}CH_3^{13}CH_2OH$ with the previously formed ^{12}C-reactive intermediates. The time evolution of relative ^{13}C content of the typical products were monitored and presented in Fig. 4. ^{13}C content of ethene is higher than other products at 250 °C and 350 °C as shown in Fig. 4(a) and 4(b), and rapidly reaches more than 90% at 350 °C. Prolonging the ^{13}C-ethanol feeding time, the incorporation content of ^{13}C atom in both effluent products and trapped organic species gradually increases. Combined with the reaction results (Fig. 1), it proves that the formation mechanism of ethene is different from that of other olefins. Among the trapped organics, three kinds of reactive intermediates identified by 2D ^{13}C–^{13}C INADEQUATE experiment and GC–MS analysis, 3,4-dimethyl-2-ethylcyclopenta diene (neutral form of cation **IV**), 2,3,4,5-tetramethyl-cyclopenta diene (neutral form of cation **I**), and 1-methyl-3,5-diethylbenzene exhibit relatively higher ^{13}C contents than other components in the $^{12}C/^{13}C$-ethanol isotope switching experiments at 250 °C. The detailed ^{13}C distribution of these species were also presented in Fig.S15-17, after switching ^{12}C-ethanol to ^{13}C-ethanol, ^{13}C was incorporated in 1,2,3,4-tetraMCP, 4,5-DiM-3-ECP and 1-methyl-3,5-diethylbenzene. These results demonstrate the high activity of these organic species as the HCP species of ethanol reaction and confirm that the captured reactive intermediates are involved in olefins generation. Increasing the temperature to 450 °C, aromatic species appear in the effluent products, and cyclopentadiene species become undetectable among the extracted organics in catalyst. It can be deduced that the high temperature reaction accelerated the transformation of cyclopentadiene species to alkylbenzenes and polycyclic aromatics.

More detailed information about isotopic distribution of ethene and propene is presented in Fig. 4(d-f). After switching to ^{13}C-ethanol, ethene molecules without ^{13}C-labeling and the total ^{13}C-labeling dominate, but almost no ethene is incorporated with single ^{13}C atom at 250 °C. Meanwhile the proportion of total ^{13}C-labeled ethene increases significantly with the increase of reaction temperature. It indicates that ethene is most likely to be obtained directly from ethanol dehydration, which is consistent with the predominant ethene generation at 250 °C (Fig. 1). However, the isotopic distribution of propene is sensitive to temperature. At relatively lower temperatures (250 and 350 °C), the isotopic distribution of propene varies from none ^{13}C-labeled to total ^{13}C-labeled, which means part of propene is produced by the $^{13}CH_3^{13}CH_2OH$ reaction with ^{12}C-labeled HCP intermediate species, contributing to a wide ^{13}C atom distribution in propene. This result gives sufficient evidence for indirect mechanism in ETH process with the participation of some retained organics, such as cyclopentenyl cations and aromatics. While increasing temperature to 450 °C, the isotopic distribution of propene exhibited a dominating total ^{13}C incorporation at 450 °C. On the one hand, it shows that the high temperature accelerates the secondary reactions of the produced ^{13}C-labeled ethene. On the other hand, it can be speculated that the propene is mainly produced by the cracking of the ^{13}C-labeled oligomeric olefins, which originated from ^{13}C-ethene polymerization, since the cracking at high temperature becomes energetically preferable [45,46]. In addition, the reducing of the selectivity of C_{1-4} alkanes at 450 °C (Fig. 1) also illustrates the depression of the H-transfer reactions in whole reaction process, indicating a decreasing role of the aromatics-based cycle mechanism in ETH process. Moreover, the similar isotopic distribution of butenes, pentenes and propene at 450 °C (seen in Fig. S18) further demonstrates the temperature-modulated reaction route for in ETH process. These results, all together, prompt us to speculated that the ethylation-cracking mechanism in the ETH process becomes predominant at high reaction temperature (450 °C).

In general, switching experiments of ^{13}C-ethanol at different temperatures revealed the participation of the captured ethyl-substituted cyclopentenyl cations and aromatics in ETH process.

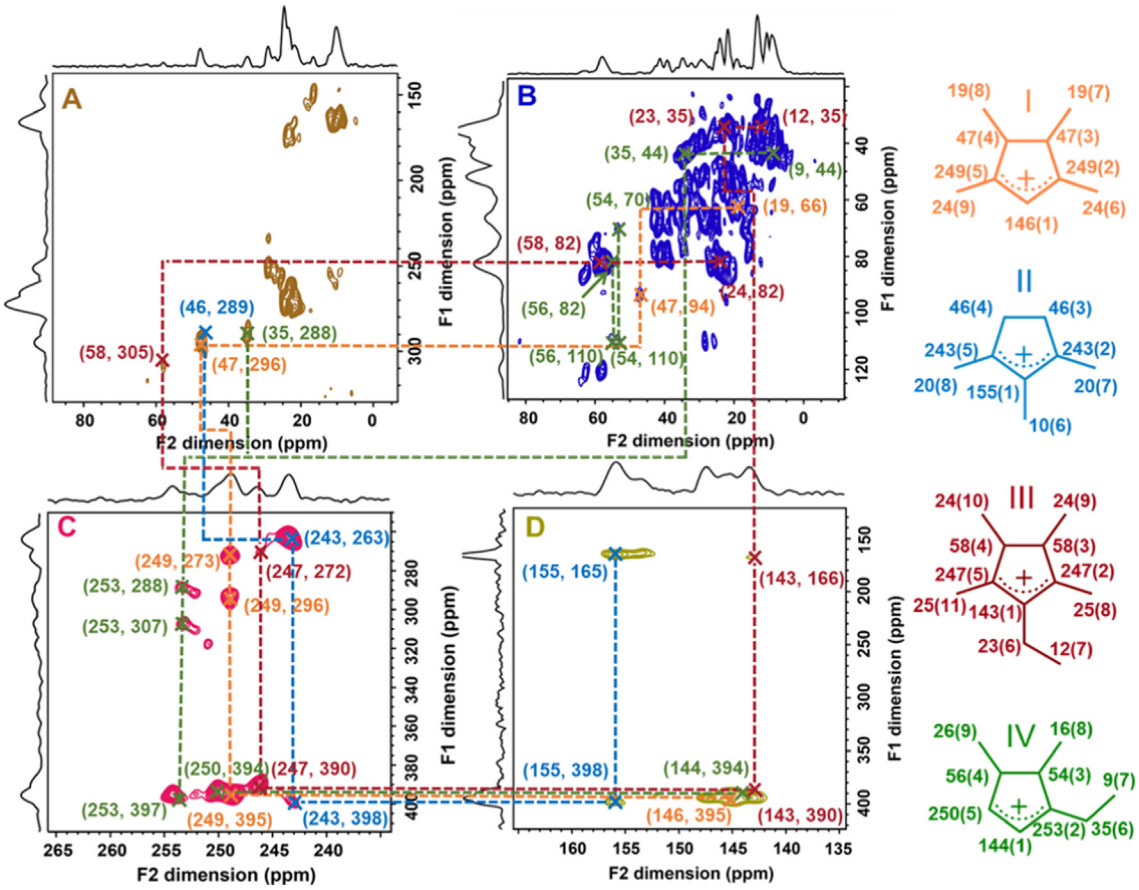

Fig. 3. Advanced 2D ^{13}C–^{13}C INADEQUATE experiment at room temperature probing trapped carbocations of $^{13}CH_3^{13}CH_2OH$ conversion. The assignments of the different carbenium ions are highlighted in different colors.

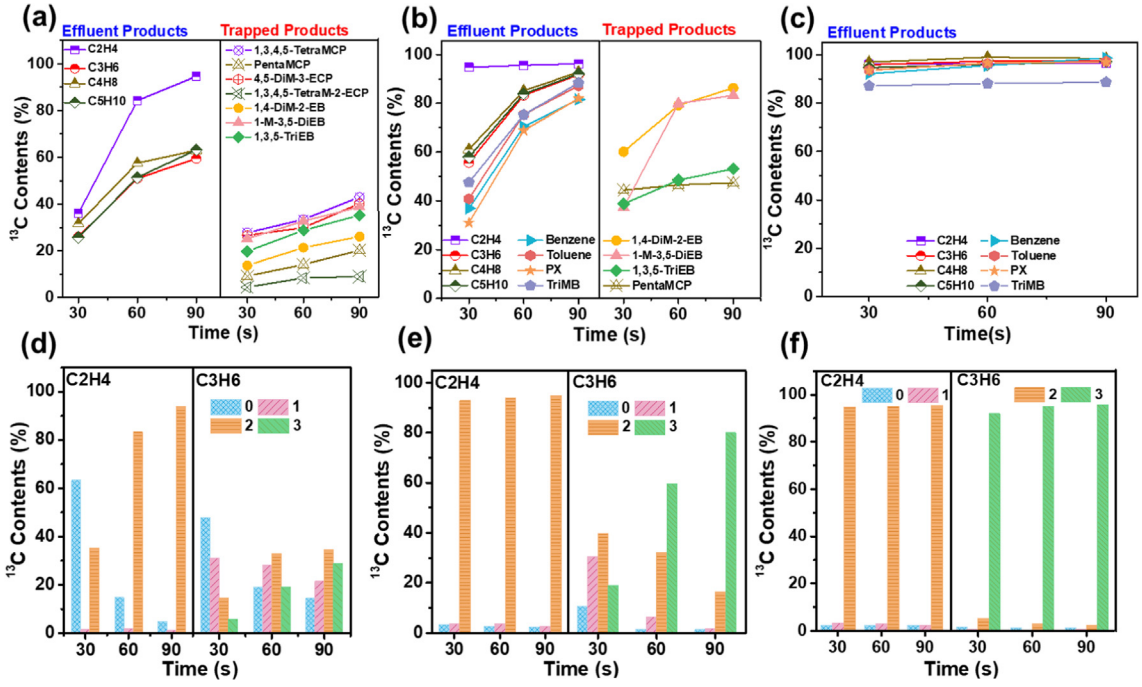

Fig. 4. Relative ^{13}C content of the effluent and the trapped products in H-ZSM-5 zeolite after ^{12}C-ethanol reaction for 15 min followed by switching to $^{13}CH_3^{13}CH_2OH$ and the isotopic distribution of ethene as well as propene at 250 °C (a), (d); 350 °C (b), (e); 450 °C (c), (f). The number 0 denotes there are no ^{13}C atom in products, number 1 denotes only one ^{13}C atom incorporated in products and so forth.

Learning from their important roles in MTH process [33], a triple-cycle reaction routes including olefins-based cycle, aromatics-based cycle, and cyclopentadienes-based cycle can be proposed to involved in the formation of the light olefins in ETH process. Furthermore, a temperature-modulated mechanism in ETH process can also be unraveled from the foregoing analyses. At low reaction temperature (ie, 250 and 350 °C), three kinds of cycle mechanism should be co-existed and worked comparatively, while higher temperature (ie, 450 °C) may make the reaction mechanism more favorable for olefin ethylation-cracking mechanism. More importantly, the formation of ethene is principally through direct dehydration of ethanol, while the formation of propene is more likely going through indirect pathway, which consolidates the existence of the cyclic organics-mediated mechanism. Meanwhile, the olefins-based cycle mechanism cannot be ruled out in ETH process. Moreover, the high activity of the cyclopentadiene species may also inspired us to propose the cyclopentadienes-based cycle for light olefins formation.

3.5. Multi-routes with the participation of different intermediate species for ethene and propene formation via DFT calculations

Based on the aforementioned results, HCP species such as 2,3,4,5-tetramethylcyclopentenyl cation (**I**), 1,2,5-trimethylcyclopentenyl cation (**II**), 2,3,4,5-tetramethyl-1-ethylcy clopentenyl cation (**III**) and 3,4-dimethyl-2-ethylcyclopentenyl cation (**IV**), were captured in ETH process via 2D ^{13}C–^{13}C INADEQUATE experiment, and more importantly, their deprotonated species (corresponding cyclopentadienes) and ethylbenzenes exhibit higher reactivity in $^{12}C/^{13}C$-ethanol isotope switching experiments at the temperature range of 250–350 °C. This means that besides direct ethanol dehydration reaction, the generated alkene products, especially propene may be produced via indirect reaction mechanism with the participation of these active intermediates. It is widely known that these intermediates are regarded as active HCP species for olefins formation in MTH reaction [13,19,39], while their roles have not been suggested in ETH process so far. These findings in the present work prompt us to propose the multi-routes with the participation of different intermediates for ethene and propene formation via indirect mechanism in ETH process over H-ZSM-5 (Fig. 5). To testify the roles of these intermediate species, DFT calculations were employed to evaluate the feasibility and the contribution of all the potential routes from energetic perspective. Computational details are provided in experimental section.

In the ETH process, when ethanol dehydrates to form ethene, HCP species accumulate in H-ZSM-5 via a series of secondary reactions, such as oligomerization, cyclization, H-transfer, and aromatization as concluded from above experimental results. These HCP species including alkenes, aromatics and cyclopentadiene species are supposed to react with ethanol to fulfill the propagation of side-chains of the cyclic and alkenyl species, and then split off olefins. In this work, starting from these active intermediates, triple-cycle routes the feasibility of ethene and propene formation process, via critical reaction steps, such as ethylation, cracking or elimination as the important elementary steps, were considered and evaluated. The critical reaction steps of the triple-cycle routes for ethene and propene formation from ethanol conversion are proposed and the associated the Gibbs free energy barriers of ethanol conversion of 250 °C, are shown in Fig. 5. Based on the observed cyclopentenyl cations (cation **I**/**II**/**III**) and dimethyl/tetramethyl cyclopentadienes with high activity, the role of these species was presented via the reaction route of cyclopentadienes-based cycle, which is found to be responsible for olefins formation in the MTH reaction system, in parallel with the olefins-based and aromatics-based cycles [34]. Starting from dimethyl/tetramethyl cyclopentadienes (1,2-dimethyl and 1,2,3,4-tetramethyl cyclopentadienes), dimethyl/tetramethyl cyclopentadienes can be ethylated with ethanol to form ethylcyclopentenyl cation (C1a, C2a), which can produce ethene and dimethyl/tetramethyl cyclopentadienes by elimination reaction (C1b, C2b). In addition, the $^{12}C/^{13}C$-ethanol isotope switching experiments confirm that the interaction of ethanol and ethyl-substituted benzenyl species can produce olefin products via aromatics-based cycle. The formation of ethyl-substituted benzenyl species and its role in ethene and propene formation is suggested in the calculation. Firstly, toluene ethylates with ethanol to form ethyl-methylbenzene (A1), which can form diethyl-methylbenzene through continuous ethylation reaction (A2). Then ethene is split off via cyclohexadiene carbenium ions (A3 and A4). For the reaction route of ETH process following the olefins-based cycle, alkoxides or carbenium ions can be easily produced via dimerization reaction, ethylation and isomerization, and then ethene is formed via a cracking reaction of long-chain alkenes, such as hexene. In this work, olefins-based cycle starting from C_{6+} were investigated in parallel with cyclopentadienes-based cycle and aromatics-based cycle.

For propene formation, triple-cycle mechanism is also suggested and theoretically evaluated. In cyclopentadienes-based cycle, 1,2,3,4-tetramethylcyclopentenyl cation is deprotonated to form trimethylmethylenecyclopentene (TMMCP) with an exocyclic double bond (C1′). Then 2,3,4-trimethyl-1-propylcyclopentenyl cation is formed via an exocyclic ethylation step (C2′). From this cation, as propene precursor, propene eliminates (C3′). Similarly, in aromatics-based cycle, when 3,5-diethyl-1-methylbenium cation forms, it loses a proton (A3′) to form 3,5-diethylmethylene cyclohexadiene (DEMC) with an exocyclic double bond. Then the propene precursor with propyl side-chain is generated via the ethylation of DEMC (A4′), followed by the propene formation via elimination reaction (A5′). In the olefins-based cycle, the function of olefins species is calculated and revealed by evaluating the cracking reaction of C_{6+} to propene (O1′).

The Gibbs free energy barrier at 250 °C for ethene and propene formation via various reaction pathways with the participation of different HCP species in ETH over H-ZSM-5 are provided in Table S1. The optimized transition state structures for ethene and propene formation via various reaction pathways with the participation of different HCP species in ETH over H-ZSM-5 are shown in Fig. S19 and Fig. S20 in SI. As shown in Fig. 5, in the cyclopentadienes-based route, the free energy barriers of critical step for ethene formation from dimethyl cyclopentadiene as intermediate of 31.2 (C2b) kcal/mol are found to be lower than that from tetramethyl cyclopentadiene as the intermediate of 37.1 (C1a) kcal/mol, which is ascribed to the space limit of the bulk ethene precursor in zeolite framework. In the same way, the formation of the bulk ethylbenzene precursor needs overcome relatively higher barrier of 34.0 kcal/mol (A1) and 33.8 kcal/mol (A2), which becomes the pivotal step in the aromatics-based route. Besides, the free energy barriers of ethene formation from the cracking reaction of C_{6+} in the olefins-based route is 30.4 kcal/mol. Compared with the critical step of ethene formation through different reaction routes, it can be concluded that ethene formation from cyclopentadienes-based reaction route (31.2 kcal/mol) and olefin species-based reaction route (30.4 kcal/mol) has close free energy barrier, suggesting parallel contribution of cyclopentadienes-based and olefins-based cycle for ethene formation in ETH process. Therefore, combined with the experimental results discussed above, although the majority of ethene can be generated from direct dehydration of ethanol, HCP species also can play their important roles in the formation of ethene.

Furthermore, the feasibility of the triple-cycle routes for propene formation was evaluated. In the cyclopentadienes-based route, relative lower barriers of 15.9–20.6 kcal/mol are predicted for propene formation, where an ethylation reaction with free bar-

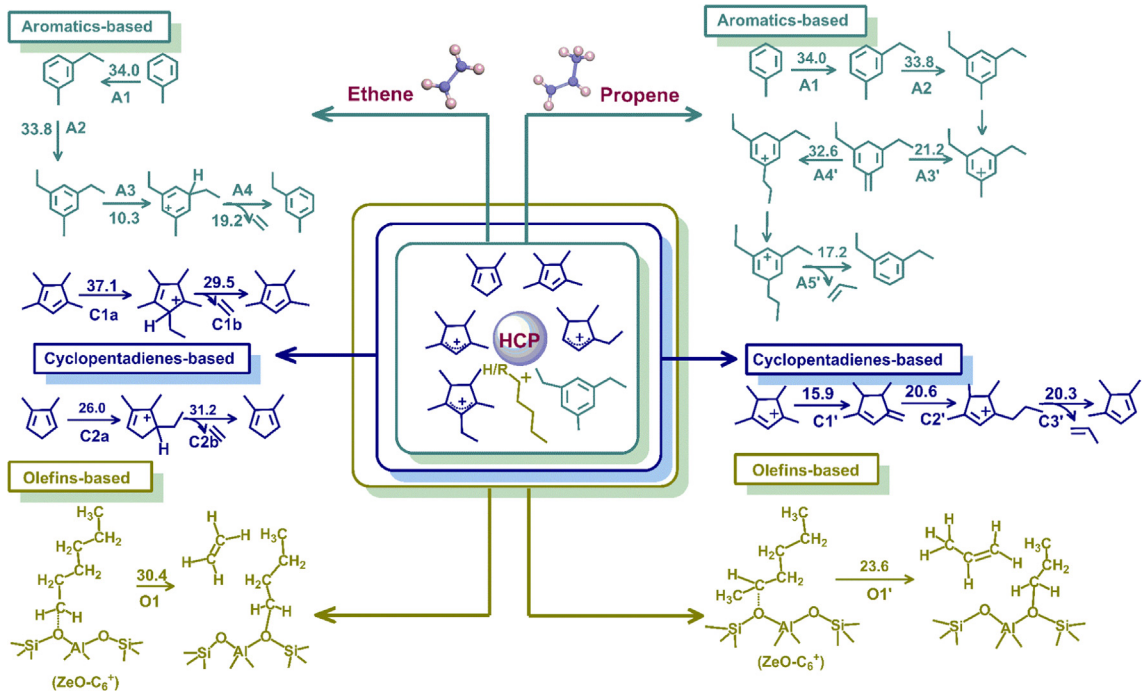

Fig. 5. Ethene and propene formation via triple-cycle routes with the participation of different intermediate species in ETH over H-ZSM-5. Calculated free energy barriers at 250 °C are given in kcal/mol.

rier of 20.6 kcal/mol (C2′) is slightly lower than the cracking reaction of C_{6+} (23.6 kcal/mol, O1′) in olefins-based route. When the 3,5-diethyl-1-methylbenzenium cation forms, the ethylation reaction of DEMC also needs to overcome relative high barrier of 32.6 kcal/mol (A4′), owing confinement effect from zeolite environment. This means that ethylation reactions (A1, A2, A4′) are the critical steps for the propene formation via aromatics-based route. That is, compared to the aromatics-based route, cyclopentadienes-based and olefins-based routes with the participation of cyclopentadienes and olefins species favor the propene formation. It is worth noting that the free energy barriers for propene formation via cyclopentadienes-based route (20.6 kcal/mol, C2′) and olefins-based (23.6 kcal/mol, O1′) route are obviously lower by 6.8–10.5 kcal/mol than that of ethene formation with 31.2 kcal/mol (C2b) and 30.4 kcal/mol (O1), respectively. These results demonstrate that HCP species can function a significant role in olefins formation in ETH process, in which cyclopentadienes, aromatics and olefins species are the dominant active intermediates. Furthermore, relative lower free barrier of propene formation suggests that the reaction route mediating by HCP species favors the propene production in ETH process.

4. Conclusion

In conclusion, the detailed mechanism of ethanol conversion was studied by the multiple experimental methods and DFT calculation. In situ ^{13}C MAS NMR spectroscopy recorded the whole reaction process under real-time condition. Ethanol experienced a dehydration stage firstly to form ethene. Thereafter, ethene quickly transformed to active cyclopentenyl cations and aromatics via oligomerization, cyclization and aromatization reactions. Especially, four cyclopentenyl cations with methyl or ethyl substituted were explicitly identified by 2D ^{13}C–^{13}C INADEQUATE NMR experiment. Subsequently, these cyclopentenyl cations and aromatics such like 3,4-dimethyl-2-ethylcyclopentenyl cation, 2,3,4,5-tetra methyl-cyclopentenyl cation and 1-methyl-3,5-diethylbenzene presented high activity in ^{13}C-isotope switching experiments and were suggested to be the active HCP species in ETH process. Moreover, ethene was supposed primarily to be generated through direct dehydration of ethanol. These captured HCP species were further proved to play a significant role in olefins formation especially propene formation in ETH process by DFT calculation. Finally, a triple-cycle route including olefins-based, aromatics-based and cyclopentadienes-based routes, which were reported in MTH process, were also proposed to reveal the formation pathway of ethene and propene in ETH process. In addition, the reaction routes were speculated sensitive to temperature. At low reaction temperature (ie, 250 and 350 °C), the three kinds of cycles work together in parallel for olefins formation. However, the olefins ethylation-cracking mechanism gradually become a dominant route at higher temperature (ie, 450 °C). These findings not only provide the detailed mechanism of ETH process, but also are of great importance for enriching the fundamental understandings of the alcohol's conversion.

Declaration of Competing Interest

The authors declare that they have no known competing financial interests or personal relationships that could have appeared to influence the work reported in this paper.

Acknowledgements

This work was supported by the National Natural Science Foundation of China (22022202, 22002157, 21972142, 21991092, 21991090), the National Key R&D Program of China (No. 2021YFA1502600), Dalian Outstanding Young Scientist Foundation (2021RJ01), the Key Research Program of Frontier Sciences, Chinese Academy of Sciences (QYZDY-SSW-JSC024), International Partnership Program of Chinese Academy of Sciences (121421KYSB20180007).

Appendix A. Supplementary material

Supplementary data to this article can be found online at https://doi.org/10.1016/j.jcat.2022.07.002.

References

[1] J. Sun, Y. Wang, ACS Catal. 4 (2014) 1078–1090.
[2] O.J. Sanchez, C.A. Cardona, Bioresource Technol. 99 (2008) 5270–5295.
[3] M. Boronat, C.M. Sánchez, D. Law, A. Corma, J. Am. Chem. Soc. 130 (2008) 16316–16323.
[4] H. Xin, X. Li, Y. Fang, X. Yi, W. Hu, Y. Chu, F. Zhang, A. Zheng, H. Zhang, X. Li, J. Catal. 312 (2014) 204–215.
[5] A.G. Gayubo, A. Alonso, B. Valle, A.T. Aguayo, M. Olazar, J. Bilbao, Fuel 89 (2010) 3365–3372.
[6] Z. Song, A. Takahashi, I. Nakamura, T. Fujitani, Appl. Catal. A-Gen. 384 (2010) 201–205.
[7] W.R. Moser, R.W. Thompson, C. Chiang, H. Tong, J. Catal. 117 (1989) 19–32.
[8] Z. Song, A. Takahashi, N. Mimura, T. Fujitani, Catal. Lett. 131 (2009) 364–369.
[9] K. Van der Borght, R. Batchu, V.V. Galvita, K. Alexopoulos, M.F. Reyniers, J.W. Thybaut, G.B. Marin, Angew. Chem. Int. Ed. 55 (2016) 12817–12821.
[10] A.D. Chowdhury, A.L. Paioni, G.T. Whiting, D. Fu, M. Baldus, B.M. Weckhuysen, Angew. Chem. Int. Ed. 58 (2019) 3908–3912.
[11] A. Takahashi, W. Xia, Q. Wu, T. Furukawa, I. Nakamura, H. Shimada, T. Fujitani, Appl. Catal. A-Gen. 467 (2013) 380–385.
[12] R. Johansson, S.L. Hruby, J. Rass-Hansen, C.H. Christensen, Catal. Lett. 127 (2009) 1–6.
[13] S. Xu, A. Zheng, Y. Wei, J. Chen, J. Li, Y. Chu, M. Zhang, Q. Wang, Y. Zhou, J. Wang, F. Deng, Z. Liu, Angew. Chem. Int. Ed. 52 (2013) 11564–11568.
[14] X. Wu, S. Xu, W. Zhang, J. Huang, J. Li, B. Yu, Y. Wei, Z. Liu, Angew. Chem. Int. Ed. 56 (2017) 9039–9043.
[15] S. Svelle, F. Joensen, J. Nerlov, U. Olsbye, K.-P. Lillerud, S. Kolboe, M. Bjørgen, J. Am. Chem. Soc. 128 (2006) 14770–14771.
[16] C. Wang, Q. Wang, J. Xu, G. Qi, P. Gao, W. Wang, Y. Zou, N. Feng, X. Liu, F. Deng, Angew. Chem. Int. Ed. 128 (2016) 2553–2557.
[17] Y. Liu, S. Muller, D. Berger, J. Jelic, K. Reuter, M. Tonigold, M. Sanchez-Sanchez, J.A. Lercher, Angew. Chem. Int. Ed. 128 (2016) 5817–5820.
[18] A.D. Chowdhury, K. Houben, G.T. Whiting, M. Mokhtar, A.M. Asiri, S.A. Al-Thabaiti, S.N. Basahel, M. Baldus, B.M. Weckhuysen, Angew. Chem. Int. Ed. 128 (2016) 16072–16077.
[19] W. Zhang, J. Chen, S. Xu, Y. Chu, Y. Wei, Y. Zhi, J. Huang, A. Zheng, X. Wu, X. Meng, F. Xiao, F. Deng, Z. Liu, ACS Catal. 8 (2018) 10950–10963.
[20] W. Zhang, M. Zhang, S. Xu, S. Gao, Y. Wei, Z. Liu, ACS Catal. 10 (2020) 4510–4516.
[21] S. Wang, Z. Wei, Y. Chen, Z. Qin, H. Ma, M. Dong, W. Fan, J. Wang, ACS Catal. 5 (2015) 1131–1144.
[22] M. Bjorgen, S. Svelle, F. Joensen, J. Nerlov, S. Kolboe, F. Bonino, L. Palumbo, S. Bordiga, U. Olsbye, J. Catal. 249 (2007) 195–207.
[23] U. Olsbye, M. Bjørgen, S. Svelle, K.-P. Lillerud, S. Kolboe, Catal. Today 106 (2005) 108–111.
[24] E.G. Derouane, J.B. Nagy, P. Dejaifve, J.H.C. van Hooff, B.P. Spekman, J.C. Védrine, C. Naccache, J. Catal. 53 (1978) 40–55.
[25] J.N. Kondo, K. Ito, E. Yoda, F. Wakabayashi, K. Domen, J. Phys. Chem. B 109 (2005) 10969–10972.
[26] J.N. Kondo, D. Nishioka, H. Yamazaki, J. Kubota, K. Domen, T. Tatsumi, J. Phys. Chem. C 114 (2010) 20107–20113.
[27] X. Zhou, C. Wang, Y. Chu, J. Xu, Q. Wang, G. Qi, X. Zhao, N. Feng, F. Deng, Nat. Commun. 10 (2019) 1961.
[28] A.G. Gayubo, A.M. Tarrío, A.T. Aguayo, M. Olazar, J. Bilbao, Ind. Eng. Chem. Res. 40 (2001) 3467–3474.
[29] F.F. Madeira, H. Vezin, N.S. Gnep, P. Magnoux, S. Maury, N. Cadran, ACS Catal. 1 (2011) 417–424.
[30] M. Inaba, K. Murata, M. Saito, I. Takahara, React. Kinet. Catal. Lett. 88 (2006) 135–142.
[31] S. Zeng, J. Li, N. Wang, W. Zhang, Y. Wei, Z. Liu, S. Xu, Energy Fuel. 35 (2021) 12319–12328.
[32] C. Wang, X. Yi, J. Xu, G. Qi, P. Gao, W. Wang, Y. Chu, Q. Wang, N. Feng, X. Liu, A. Zheng, F. Deng, Chem. Eur. J. 21 (2015) 1–9.
[33] D.M. McCann, D. Lesthaeghe, P.W. Kletnieks, D.R. Guenther, M.J. Hayman, V. Van Speybroeck, M. Waroquier, J.F. Haw, Angew. Chem. Int. Ed. 47 (2008) 5179–5182.
[34] W. Zhang, Y. Zhi, J. Huang, X. Wu, S. Zeng, S. Xu, A. Zheng, Y. Wei, Z. Liu, ACS Catal. 9 (2019) 7373–7379.
[35] J. Li, M. Liu, S. Li, X. Guo, C. Song, Ind. Eng. Chem. Res. 58 (2019) 1896–1905.
[36] K.R. Thurber, R. Tycko, J. Magn. Reson. 196 (2009) 84–87.
[37] C. Wang, Y. Chu, M. Hu, W. Cai, Q. Wang, G. Qi, S. Li, J. Xu, F. Deng, Angew. Chem. Int. Ed. 60 (2021) 26847–26854.
[38] Y. Chen, X. Zhao, Z. Qin, S. Wang, Z. Wei, J. Li, M. Dong, J. Wang, W. Fan, J. Phys. Chem. C 124 (2020) 13789–13798.
[39] J.F. Haw, J.B. Nicholas, W.G. Song, F. Deng, Z.K. Wang, T. Xu, C.S. Heneghan, J. Am. Chem. Soc. 122 (2000) 4763–4775.
[40] D. Fu, A.L. Paioni, C. Lian, O. van der Heijden, M. Baldus, B.M. Weckhuysen, Angew. Chem. Int. Ed. 59 (2020) 20024–20030.
[41] J. Li, Y. Wei, J. Chen, P. Tian, X. Su, S. Xu, Y. Qi, Q. Wang, Y. Zhou, Y. He, Z. Liu, J. Am. Chem. Soc. 134 (2012) 836–839.
[42] A. Lesage, M. Bardet, L. Emsley, J. Am. Chem. Soc. 121 (1999) 10987–10993.
[43] W. Dai, C. Wang, M. Dyballa, G. Wu, N. Guan, L. Li, Z. Xie, M. Hunger, ACS Catal. 5 (2014) 317–326.
[44] T. Xu, J. L. White, U. S. Patent 6743747, 2004, priority filing and PCT published February 2000.
[45] C.J. Chen, S. Rangarajan, I.M. Hill, A. Bhan, ACS Catal. 4 (2014) 2319–2327.
[46] R.J. Quann, L.A. Green, S.A. Tabak, F.J. Krambeck, Ind. Eng. Chem. Res. 27 (1988) 565–570.